Multimodel projections of climate change from short-lived emissions due to human activities

Drew T. Shindell,[1] Hiram Levy II,[2] M. Daniel Schwarzkopf,[2] Larry W. Horowitz,[2] Jean-Francois Lamarque,[3] and Greg Faluvegi[1]

Received 25 June 2007; revised 21 November 2007; accepted 6 February 2008; published 6 June 2008.

[1] We use the GISS (Goddard Institute for Space Studies), GFDL (Geophysical Fluid Dynamics Laboratory) and NCAR (National Center for Atmospheric Research) climate models to study the climate impact of the future evolution of short-lived radiatively active species (ozone and aerosols). The models used mid-range A1B emission scenarios, independently calculated the resulting composition change, and then performed transient simulations to 2050 examining the response to projected changes in short-lived species and to changes in both long-lived and short-lived species together. By 2050, two models show that the global mean annual average warming due to long-lived GHGs (greenhouse gases) is enhanced by 20–25% due to the radiatively active short-lived species. One model shows virtually no effect from short-lived species. Intermodel differences are largely related to differences in emissions projections for short-lived species, which are substantial even for a particular storyline. For aerosols, these uncertainties are usually dominant, though for sulfate uncertainties in aerosol physics are also substantial. For tropospheric ozone, uncertainties in physical processes are more important than uncertainties in precursor emissions. Differences in future atmospheric burdens and radiative forcing for aerosols are dominated by divergent assumptions about emissions from South and East Asia. In all three models, the spatial distribution of radiative forcing is less important than that of climate sensitivity in predicting climate impact. Both short-lived and long-lived species appear to cause enhanced climate responses in the same regions of high sensitivity rather than short-lived species having an enhanced effect primarily near polluted areas. Since short-lived species can significantly influence climate, regional air quality emission control strategies for short-lived pollutants may substantially impact climate over large (e.g., hemispheric) scales.

Citation: Shindell, D. T., H. Levy II, M. D. Schwarzkopf, L. W. Horowitz, J.-F. Lamarque, and G. Faluvegi (2008), Multimodel projections of climate change from short-lived emissions due to human activities, *J. Geophys. Res.*, *113*, D11109, doi:10.1029/2007JD009152.

1. Introduction

[2] The largest contributor to climate change since the industrial revolution has been the increased abundance of the well-mixed or long-lived greenhouse gases (GHGs) in the atmosphere. These gases are also likely to dominate future climate change. However, aerosols and ozone also play important roles in human-induced climate change. These species are now routinely included in model simulations and expert assessments of past climate change, but their future impact has received much less attention. For example, the climate models providing input to the recently completed Fourth Assessment Report (AR4) of the Intergovernmental Panel on Climate Change (IPCC) included a wide variety of detail in their projections of future aerosols and ozone, from no changes to fully time-evolving for at least some species [*Intergovernmental Panel on Climate Change*, 2007]. Even the latter models had limited representation of some processes, such as the aerosol indirect effect (AIE) or two-way coupling of aerosols and ozone with climate. Furthermore, they generally did not isolate the impacts of short-lived species from those of the long-lived GHGs. Thus the extent to which short-lived species may contribute to future climate change is unclear. Additionally, since these species are unevenly distributed, it is not clear how their changes may influence regional climate change. Hence it is important to quantify their contribution to future climate change.

[3] There are several additional reasons to emphasize short-lived species. Many of these species are pollutants that cause substantial harm to humans, crops and natural ecosystems (e.g., ozone and fine particles). Thus controls on these species could provide health benefits in addition to potentially mitigating climate change. The effects of policies

[1]NASA Goddard Institute for Space Studies, New York, New York, USA.
[2]NOAA Geophysical Fluid Dynamics Laboratory, Princeton University, Princeton, New Jersey, USA.
[3]Atmospheric Chemistry Division, National Center for Atmospheric Research, Boulder, Colorado, USA.

0148-0227/08/2007JD009152

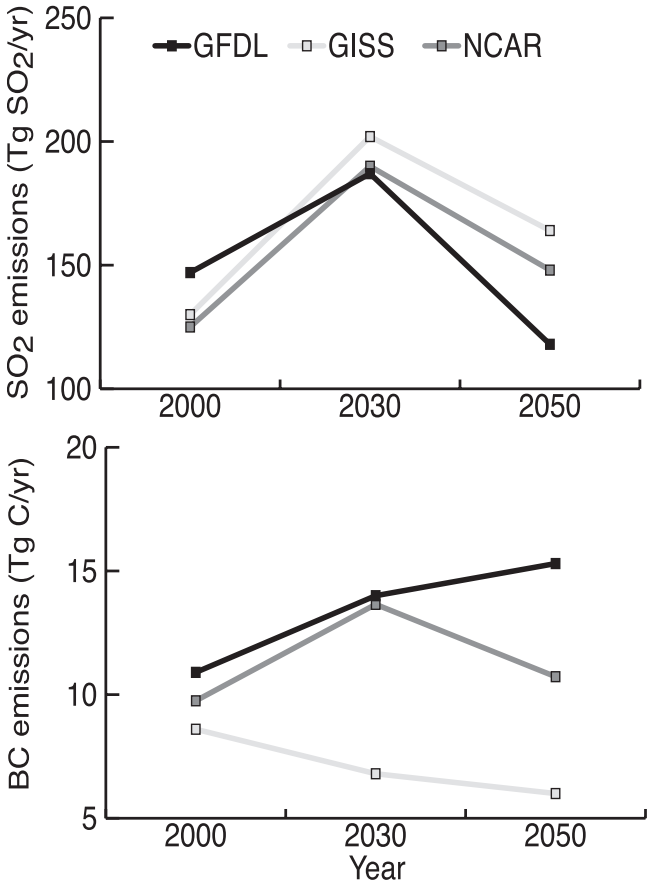

Figure 1. Emissions trends used in the three models for SO_2 (top) and BC (bottom) following the A1B storyline. Note that in the NCAR model, the present-day black carbon distribution was scaled in the future rather than calculating future amounts from BC emissions. Scaling followed the global sulfur-dioxide emissions, a 40% increase over 2000 at 2030 and 10% at 2050. The NCAR 2000 black carbon global emission is set at the average of the GISS and GFDL 2000 values, and follows this scaling in the future, for illustrative purposes.

to limit emissions of ozone and aerosol precursors would also be felt much more quickly than for long-lived GHGs given their comparatively short atmospheric lifetimes. Finally, short-lived species are known to have a large effect in the Arctic, with studies showing that there may be substantial warming there from aerosols [*Hansen and Nazarenko*, 2004; *Jacobson*, 2004; *Garrett and Zhao*, 2006] and from ozone [*Shindell et al.*, 2006a]. Given the dramatic changes already taking place there, and the potential catastrophic consequences of Greenland Ice Sheet melting or release of methane from thawing permafrost, it is crucial to better understand what controls future warming trends in that region.

[4] Given the scientific importance of better understanding the magnitude, spatial distribution, and timing of future warming due to short-lived species, and the lack of previous results, we undertook a multimodel experiment to investigate this topic. This work was carried out as part of the United States Climate Change Science Program (CCSP) in support of Synthesis and Assessment Product 3.2 "Climate Projections Based on Emiss cenarios for Long-lived and Short-lived Radiatively Active Gases and Aerosols". The work described here constitutes a large portion of the assessment of the impact of short-lived species in that report. We note also that these new simulations were intended to compliment those performed for the IPCC AR4, and in fact to aid in their interpretation. Hence rather than prescribing identical emissions in the models, we use the same short-lived and long-lived species projections for GFDL and NCAR as in AR4, and for GISS use the same long-lived species and now also include short-lived species. This allows us to isolate the relative influence of the short- and long-lived species in these models' AR4 projections.

[5] Several steps are involved in projecting climate change due to human activities. First, projections of emissions of radiatively active species and their precursors are created using Integrated Assessment Models (IAMs) based on a socio-economic development scenario. Next, the atmospheric abundances of these species must be calculated based on the projected emissions. For many species, especially long-lived GHGs, the IAMs themselves project future concentrations. For short-lived species, full three-dimensional atmospheric composition models are usually used. Last, global climate models (also called atmosphere ocean general circulation models (AOGCMs)) are used to simulate the climate response to the abundance changes. We examine the role of all three of these steps in this study. In this paper, we follow the order of this process. Section 2 describes the emission scenarios and composition models used, section 3 describes and compares the concentration projections of the models, section 4 describes the climate experiments and models, section 5 gives results of the transient climate simulations, and conclusions are presented section 6.

2. Emission Scenarios and Composition Model Descriptions

2.1. Short-Lived Species Emission Scenarios

[6] Though the three models all prescribed future emissions nominally following the A1B scenario, they used different emissions trends. There are several reasons for the differences. For one, the emissions projections only provide estimates of anthropogenic emissions, and each model used its own natural emissions (though these were largely held constant). Secondly, numerous IAM groups used the A1 socio-economic storyline to drive their models, providing a range of results to the IPCC Special Report on Emission Scenarios (SRES) [*Nakicenovic et al.*, 2000]. The GFDL and NCAR models used output from the AIM model while GISS used results from the IMAGE model. Though the AIM models output was denoted the "marker" scenario, the SRES noted that these do not represent the average, best, or median results, and that all IAM results should be treated equally. The IMAGE model projects slower economic growth than the AIM model. Total energy use is also different in the two models, with 3% greater use in the IMAGE model by 2030, but 9% less usage at 2050. The IMAGE model is less optimistic about emissions controls, leading to greater emissions than in the AIM model for the long-lived gases. For short-lived species, the original SRES A1 IMAGE sulfur oxide (SO_x) emissions were much larger than those of the AIM (or most any other) model (Figure 1). However, the revised IMAGE values used here are quite similar.

Table 1. Global Emissions[a]

Species	Model	2000	2030	2050	2100
NOx (Tg N/a)	GFDL	40	57 (43%)	54 (35%)	48 (20%)
	GISS	50.5	67.0 (33%)	77.5 (53%)	NA
BC (Tg C/a)	GFDL	10.9	14.0 (28%)	15.3 (40%)	19.9 (83%)
	GISS	8.6	6.8 (−21%)	6.0 (−30%)	NA
OC (Tg C/a)	GFDL	51.5	61.9 (20%)	66.5 (29%)	84.3 (64%)
	GISS	69.5	57.0 (−18%)	58.3 (−16%)	NA
SO_2(Tg SO_2/a)	GFDL	147	187 (27%)	118 (−20%)	56 (−62%)
	GISS	130	202 (55%)	164 (26%)	NA
	NCAR	125	190 (52%)	148 (18%)	NA
Dust (Tg/a)	GFDL	2471	2471	2471	2471
	GISS	1580	1580	1580	NA

[a]Emissions from both anthropogenic and natural sources are included. Values in parentheses are changes relative to 2000.

[7] Additionally, emissions for some species, such as carbonaceous aerosols, were not provided by the IAMs. This last issue motivated the GISS choice of the IMAGE model output, as this model provided sufficient regional detail to allow carbonaceous emissions to be estimated consistently with the other species. Another complexity was the treatment of biomass burning emissions, which are partly natural and partly anthropogenic. In the GFDL model, these were assumed to be half natural and half anthropogenic, with the latter portion following the projections for other anthropogenic sources. The GISS model instead used biomass burning emissions projections from *Streets et al.* [2004].

[8] The result is a substantial divergence in the projected trends among the three models (Figure 1 and Table 1). For sulfur-dioxide (SO_2), the emissions follow reasonably similar trajectories, with globally averaged increases until 2030 followed by decreases to 2050. The percentage increase is roughly twice as large in the GISS and NCAR models as in the GFDL model, however. Thus even the GFDL and NCAR models using projections from the same IAM show large differences in their emissions pathways, presumably owing to the treatment of natural and biomass burning emissions. At 2050, the emissions in the GFDL model are substantially reduced compared with 2000, while the other models show enhanced emissions relative to 2000 at this time. Differences are even more striking for carbonaceous aerosols. We focus on black carbon (BC) as the more important radiative perturbation. For this aerosol (and for organic carbon (OC)), the GFDL model uses the IPCC Third Assessment Report (TAR) recommendation to scale anthropogenic carbonaceous aerosol emissions according to carbon monoxide (CO), leading to substantial increases with time (Figure 1 and Table 1). At 2050, emissions increase 38% following the CO trajectory in the AIM model, with a range of 8 to 119% increases in the SRES IAMs. The recommendation to scale carbonaceous aerosol emissions to CO emissions was meant to fill in a gap in the emissions provided by the IAMs. Many of the sources of carbon monoxide emissions are rather different from those of carbonaceous aerosols, however. Hence the NCAR group decided to have BC and OC follow a trajectory similar to that for SO_2. The GISS group used emissions projections from *Streets et al.* [2004] based on energy and fuel usage trends from the IMAGE model (as for other species) and including expected changes in emissions-control technology. This led to a substantial reduction in future emissions of carbonaceous aerosols. Note that NCAR did not perform simulations of future composition based on emissions for BC and OC, but instead scaled their present-day distribution by the factors given in Figure 1.

[9] For precursors of tropospheric ozone, there was again divergence among the models. Emissions of nitrogen oxides (NO_x), the primary limiting precursor in most regions, increased steadily in the IMAGE projections used by GISS, while they peaked at 2030 and decreased slightly thereafter in the AIM projections used at GFDL (Table 1). Hydrocarbons and carbon monoxide show analogous differences. Thus ozone, in addition to the aerosols, was modeled in a substantially different way at the three centers. Methane was prescribed at the A1B AIM value for chemical calculations in all three models.

[10] The three models largely included projected changes in the same species, with the exception of nitrate which varied in the GISS model only. As its contribution to the total number of fine aerosol particles ($PM_{2.5}$) or total aerosol radiative forcing (RF) is small, this has only a small effect, however.

2.2. Well-Mixed Greenhouse Gas Scenario

[11] The long-lived gases used to drive the climate models were carbon dioxide (CO_2), nitrous oxide (N_2O), methane (CH_4), and the minor species (various halocarbons, sulfur hexafluoride (SF_6)). All three models prescribed the same concentrations, using values projected for the A1B scenario by the AIM integrated assessment model, the so-called "marker" scenario for this "family" (where a family is the results of the various IAMs projecting A1B emissions and abundances). The A1B socio-economic development storyline contains a balance between fossil fuel and renewable energy sources, rapid economic growth and introduction of new and more efficient technologies, and low population growth, making it a mid-range development scenario among those in the IPCC Special Report on Emissions Scenarios [*Nakicenovic et al.*, 2000].

2.3. Composition Models

[12] The composition simulations projected short-lived gases and aerosols using the 3 groups' own chemistry-aerosol composition models run in time slices either every decade (GFDL), at 2000, 2030 and 2050 (GISS), or at 2000 and then scaled annually for the future (NCAR). The composition simulations were driven by the A1B emissions projections discussed in sections 2.1 and 2.2. The chemical composition simulations were only run for one or two years, with the seasonally varying three-dimensional monthly mean abundances and/or optical properties archived for use as off-line fields to drive the climate simulations. These simulations were all performed with present-day climate conditions.

2.3.1. NOAA Geophysical Fluid Dynamics Laboratory (GFDL)

[13] The configurations of the GFDL climate and composition models used here have been described in detail by [*Levy et al.*, 2008]. Composition changes in the GFDL experiments were calculated using the global chemical transport model MOZART-2 (Model for OZone And Related chemical Tracers, version 2.4), which has been described in detail previously [*Horowitz et al.*, 2003; *Horowitz*, 2006, and references therein]. This model was used to generate the ozone, sulfate, and black and organic carbon distributions for

the emission scenarios discussed in section 2.1. MOZART-2 includes 63 gas-phase species, 11 aerosol and precursor species to simulate sulfate, nitrate, ammonium, and black and organic carbon and 5 size bins for mineral dust. It is driven by meteorological inputs provided every three hours from the middle atmosphere version of the NCAR Community Climate Model (MACCM3) [*Kiehl et al.*, 1998].

[14] The horizontal resolution is 2.8° latitude × 2.8° longitude, with 34 hybrid sigma-pressure levels extending up to 4 hPa. Photolysis frequencies for clear-sky are interpolated from a pre-calculated lookup table, based on TUV (version 3.0) [*Madronich and Flocke*, 1998] and modified to account for cloudiness [*Brasseur et al.*, 1998], but do not account for effects of the simulated aerosols. Stratospheric concentrations of ozone and several other long-lived gases are relaxed to present-day climatological values in MOZART-2; the future recovery of stratospheric ozone is not accounted for in the GFDL simulations of tropospheric composition. The dry deposition and wet removal schemes are described in detail by *Horowitz* [2006] and references therein. In addition to scaling emissions of methane, the initial conditions for methane were scaled to match the global average methane abundances specified in the A1B-AIM scenario. Three-dimensional monthly mean distributions of short-lived species in the troposphere were archived from simulations for each decade from 2000 to 2050 and then used in the transient climate simulations. Stratospheric ozone from the MOZART simulations was not used in the GFDL climate model; instead, a present-day climatology and future polar changes were prescribed as described in section 4.1.

[15] Present-day anthropogenic emissions were based on the EDGAR inventory [*Olivier and Berdowski*, 2001] with the exception of carbonaceous aerosols, which came from *Cooke et al.* [1999], with the OC emissions doubled to account for rapidly produced secondary OC aerosols. The global burden is 0.07 Tg C for those secondary organic aerosols that are actively simulated within the model. Natural emissions were 465 Tg/a isoprene, 3 Tg N/a lightning NO_x, and 15.5 Tg S/a dimethyl sulfate (DMS).

[16] Simulated ozone concentrations agree well with present-day observations and recent trends [*Horowitz*, 2006]. Overall, the predicted present-day concentrations of aerosols are within a factor of two of the observed values and have a tendency to be overestimated [*Ginoux et al.*, 2006].

2.3.2. NASA Goddard Institute for Space Studies (GISS)

[17] The configurations of the GISS climate and composition models used here have been described in detail by *Shindell et al.* [2007]. In brief, the composition model PUCCINI (Physical Understanding of Composition-Climate INteractions and Impacts) includes ozone and oxidant photochemistry in both the troposphere and stratosphere [*Shindell et al.*, 2006b], sulfate, carbonaceous and sea-salt aerosols [*Koch et al.*, 2006; *Koch et al.*, 2007], nitrate aerosols [*Bauer et al.*, 2006], and mineral dust [*Miller et al.*, 2006a]. Most importantly, these components interact with one another, with linkages including oxidants affecting sulfate, gas-phase nitrogen species affecting nitrate, sulfate affecting nitrogen heterogeneous chemistry via reaction of N_2O_5 to HNO_3, and sulfate and nitrate being absorbed onto mineral dust surfaces (i.e., the aerosols are internally mixed as gs form on dust surfaces [*Bauer et al.*, 2006]). The simulations described here were run using a 23-layer (up to 0.01 hPa), 4° by 5° horizontal resolution version of the ModelE GCM [*Schmidt et al.*, 2006]. Present-day emissions are based on the IIASA 2000 version of the EDGAR inventory for all anthropogenic sources [*Dentener et al.*, 2005]. As secondary organic aerosols are not simulated in the model, OC from these sources is added to present-day OC emissions (based on the present-day terpene emission distribution), where it makes up ~24% of the total. Other natural emissions were 356 Tg/a isoprene, 5.6 Tg N/a lightning NO_x, and 21.3 Tg S/a DMS.

[18] Present-day composition results in the model are generally similar to those in the underlying chemistry and aerosol models documented previously, with a few exceptions. The model used here does not include the enhanced convective scavenging of insoluble species prescribed by *Koch et al.* [2007]. Therefore our carbonaceous aerosol burden, especially in the free troposphere, is nearly double that of *Koch et al.* [2007]. Agreement with the limited available observations is comparable between the two simulations (a positive bias replaces a negative bias). Three-dimensional seasonally varying distributions of short-lived species were archived and then used in the transient climate simulations. These include projected changes in stratospheric ozone, which responds to both reductions in ozone-depleting substances and also to increases in GHGs that affect local composition and temperature.

2.3.3. National Center for Atmospheric Research (NCAR)

[19] The evolution of sulfate was calculated using the MOZART model. Present-day tropospheric ozone is from *Lamarque et al.* [2005]. Both used anthropogenic emissions from the EDGAR inventory [*Olivier and Berdowski*, 2001] for the present-day. Beyond 2000, global average tropospheric ozone was calculated by T. Wigley using the MAGICC model (a model containing one land and ocean box in each hemisphere rather than the full three-dimensional composition models used by the other groups, see http://www.cru.uea.ac.uk/~mikeh/software/magicc.htm) forced by time-varying emissions of NO_x, methane and volatile organic carbons (VOCs) following the A1B AIM scenario. These tropospheric ozone values were used to scale the present-day distribution by a globally uniform factor. Present-day distributions of sulfate and carbonaceous aerosols are based on assimilate satellite data sets [*Collins et al.*, 2001]. These distributions are also used for future carbonaceous aerosols, which are created by scaling the present-day fields by a globally uniform factor whose time evolution follows the evolution of SO_2 emissions. Stratospheric ozone changes are prescribed following the study by *Kiehl et al.* [1999]. Natural emissions were 500 Tg/a isoprene, 5.0 Tg N/a lightning NO_x, and 15.5 Tg S/a DMS.

3. Concentration Projections

3.1. Tropospheric Burdens

[20] The composition models each calculate time-varying three-dimensional distributions of all the trace species (except for ozone, BC and OC for NCAR, which were scaled in the future). We compare the global annual

Table 2. Global Tropospheric Burdens[a]

Species	Model	2000	2030	2050	2100
BC (Tg C)	GFDL	0.28	0.36 (29%)	0.39 (39%)	0.51 (82%)
	GISS	0.26	0.19 (−27%)	0.15 (−42%)	NA
	NCAR		(40%)	(10%)	NA
OC[b] (Tg C)	GFDL	1.35	1.59 (18%)	1.70 (26%)	2.15 (59%)
	GISS	1.65	1.33 (−19%)	1.27 (−23%)	NA
	NCAR		(40%)	(10%)	NA
SO_4 (Tg SO_4)	GFDL	2.52	3.21 (27%)	2.48 (−2%)	1.50 (−40%)
	GISS[c]	1.51	2.01 (33%)	1.76 (17%)	NA
	NCAR		(40%)	(10%)	NA
Ozone (DU)	GFDL	34.0	38.4 (13%)	39.3 (16%)	38.2 (12%)
	GISS	31.6	41.5 (31%)	47.8 (51%)	NA
	NCAR	28.0	41.5 (48%)	43.0 (54%)	NA

[a]Values in parentheses are changes relative to 2000. Global dust burdens were 22.31 Tg in the GFDL model and 34.84 Tg in the GISS model and did not change with time.

[b]The OC burdens include primary OC aerosols (with emissions as in above table) plus secondary OC aerosols.

[c]GISS sulfate burdens include sulfate on dust surfaces, which makes up as much as $^1/_2$ the total burden.

average tropospheric burden from each of these models. As with emissions, the differences in burdens are substantial (Table 2). The GFDL model has a 67% greater present-day burden of sulfate than the GISS model (even though the GISS burden includes the sulfate on dust surfaces). The GFDL sulfur dioxide emissions were only 13% greater, however. Analyzing the atmospheric residence time (Table 3), we see that it is quite similar in the two models for sulfate, and in fact is slightly less in the GFDL model. This indicates that the conversion of sulfur dioxide to sulfate must be much more efficient in the GFDL model for it to have a sulfate burden so much larger than the GISS model's. This is clearly seen in the ratio between sulfate burden and SO_2 emissions (Table 4). This ratio can be analyzed in terms of the total sulfate burden (in Tg) per SO_2 emission (in Tg/a), the change in sulfate burden per SO_2 emission change, or alternatively the percentage change in each. The latter is probably the most useful as the fractional change will reduce differences between the models' starting points. We note that this metric is affected by both production and removal rates in the models (though given the similarity in residence times, differences in sulfate removal rates appear to be quite small). Table 4 shows clearly that the production of sulfate per Tg SO_2 emitted is much greater in the GFDL model than in the GISS model, either because of differences in other sources of sulfate (e.g., from DMS, though DMS emissions are greater in the GFDL model) or differences in the chemical conversion efficiency of SO_2 to sulfate or the physical removal of SO_2 by deposition.

[21] The BC and OC residence times are also fairly similar in these two models (Table 3). While all the aerosols are influenced by differences in how the models simulate removal by the hydrologic cycle, accounting for at least some of the 10–15% difference in carbonaceous aerosol residence times, sulfate production can vary even more from model to model as its production from the emitted sulfur-dioxide involves chemical oxidation, which can differ substantially between models. Removal of sulfur dioxide prior to conversion to sulfate may also be more efficient in the GISS model. In contrast, BC and OC are emitted directly, and hence any differences in how these are represented in the models would be apparent in their residence times.

[22] The aerosol residence times vary little with time in the GISS and GFDL models. The carbonaceous aerosol residence times decrease with time in the GISS model (and to a lesser extent in the GFDL model for OC), probably owing to the shift with time from mid to tropical latitudes, where wet and dry removal rates are different (more rapid net removal). The aerosol indirect effect in the GISS model may also play a role in the shorter future lifetimes. The sulfate residence time is fairly stable over the 2000 to 2050 period. The ratio of sulfate burden to SO_2 emissions is the same for the present-day and the 2030 to 2000 changes in the GFDL model, but appears to change markedly by 2050. For the 2100 to 2000 change in that model (not shown), this production efficiency shifts again, dropping from 1.00 to 0.65. The efficiency also varies over time in the GISS model, decreasing to 2030 and increasing slightly thereafter (inversely related to total sulfur-dioxide emissions). This may reflect both non-linearities in production (via oxidation chemistry) and the changing spatial pattern of emissions.

[23] Comparing the intermodel variations in aerosol residence times and production efficiencies with the variations in emissions trends, it is clear that the differences in the projected changes in aerosol burdens in the GISS and GFDL simulations are primarily attributable to the underlying differences in emissions. This is especially true for carbonaceous aerosols, for which the residence times are quite similar in the models. Even though there are substantial differences in sulfate due to the variations in production efficiency between the models, the emissions trends at 2050 relative to 2000 are of opposite sign in the two models and thus dominate the difference in the burden change. Thus the GISS model projects a greater sulfate burden at 2050 than at 2000, but substantially reduced burdens of carbonaceous aerosols, while the GFDL model projects the opposite, both because of the underlying emissions projections.

[24] The results for tropospheric ozone tell a different story. The ozone burden increases in the future in all three models, but the percentage increase relative to 2000 differs by more than a factor of three at 2030 (Table 2). Examining the ozone changes relative to the NO_x emissions changes, there are very large differences between the GFDL and GISS models (Table 4). This reflects the influence of processes such as stratospheric ozone influx, which are independent of NO_x emissions, as well as the role of precursors such as CO and hydrocarbons that also influence tropospheric ozone. In particular, the GISS model found a large increase in the flux of ozone into the troposphere as the stratospheric ozone layer recovered, while the composition model used at GFDL to calculate ozone held stratospheric ozone fixed and hence did not find similar large increases. In addition, there are well-known non-linearities in O_3-NO_x chemistry [*Stewart et al.*, 1977], and it has been shown that the ozone production efficiency can vary substantially with time [*Lamarque et al.*, 2005; *Shindell et al.*, 2006a]. Finally, the GISS model included interactions between the AIE and ozone, which the others did not. Thus for tropospheric ozone, the differences in modeled changes of nearly a factor of three (13 versus 31% increase) are

Table 3. Global Mean Annual Average Aerosol Residence Times (Days)[a]

Species	Model	2000	2030	2050
BC	GFDL	9.4	9.4	9.3
	GISS	11.0	10.2	9.1
OC	GFDL	9.6	9.4	9.3
	GISS	8.7	8.5	8.0
SO_4	GFDL	8.0	8.2	8.1
	GISS	8.8	8.8	9.0

[a]Note that GISS sulfate values are for gas-phase sulfate for comparison with GFDL. Sulfate on dust surfaces has a residence ~40% longer in the GISS model.

much larger than the differences in the NO_x precursor emissions (33 versus 43% increase).

3.2. Aerosol Optical Depth

[25] The global mean present-day all-sky aerosol optical depth (AOD) in the three models ranges from 0.12–0.20 (Table 5). This is a very large range, and suggests that aerosols are contributing quite differently to the Earth's energy balance with space in these models. Observational constraints on the all-sky value are not readily available, as most of the extant measurement techniques are reliable only in clear-sky (cloud-free) conditions. Sampling clear-sky areas only, the GISS model's global total AOD is 0.12 for 2000 (0.13 Northern Hemisphere (NH), 0.10 Southern Hemisphere (SH)). This includes contributions from sulfate, carbonaceous, nitrate, dust, and seasalt aerosols. Clear-sky observations give global mean values of ~0.135 (ground-based AERONET) or ~0.15 (satellite composites), though these have substantial limitations in their coverage [*Kinne et al.*, 2006]. The NCAR and GFDL models did not calculate clear-sky AOD. Given that the all-sky values are larger, and substantially so in the GISS model (though this will depend upon water uptake by aerosols), it seems clear that the values for NCAR would be too small compared with observations since even their all-sky values are lower than the estimate from observations. This may be related to the assimilation of AVHRR data in the creation of the climatology used for present-day aerosols by NCAR [*Collins et al.*, 2001, 2006], as that data appears to be low relative to MODIS observations, for example.

[26] There are also large differences in the relative contributions of the various aerosol species in the models (Figure 2 and Table 5). This is true even for the GFDL and GISS models, with relatively similar all-sky global mean AODs. More than half the AOD in the GFDL model comes from sulfate, while this species contributes only about 1/8th the AOD in the GISS model. Instead, the GISS model's AOD is dominated by the largely natural sea-salt and dust aerosols, which together contribute 0.14 (74%) to the AOD. These two species contribute a much smaller AOD in the NCAR and GFDL models, ~0.06 or less, with the differences with respect to GISS predominantly due to sea-salt. The relative contribution from sulfate in the NCAR model looks similar to the GFDL model, with nearly half its AOD coming from sulfate, but the magnitude is much smaller. It seems clear that the GFDL model's direct sulfate contribution is biased high [*Ginoux et al.*, 2006], while the GISS model's sulfate is biased low in this model version [*Shindell et al.*, 2007]. However, the relative importance of the different aerosol species is not well understood at present [*Kinne et al.*, 2006].

[27] Large differences in the AOD between the NH and SH are also apparent in the models (Table 5). The total present-day NH/SH AOD ratios in the three models differ widely, at 2.43, 1.97, and 0.96 in the GFDL, NCAR, and GISS models, respectively. The clearly reflects the dominant role of sulfate in the GFDL and NCAR models, as this species has large anthropogenic NH sources, and the dominance of sea-salt in the GISS model, with its largest source being the Southern Ocean. While composite satellite data shows clearly greater clear-sky AODs in the NH than the SH, most satellite instruments lose coverage near the northern edge of the Southern Ocean [*Kinne et al.*, 2006]. Unfortunately, quality-controlled networks such as AERONET provide virtually no ground-based data poleward of 45°S. Thus while it seems that a greater all-sky AOD in the SH than the NH, as in the GISS model (though this model had a greater clear-sky AOD in the NH than the SH), might be unlikely, current data are not adequate to fully characterize this ratio as AODs over the Southern Ocean are poorly known.

4. Climate Simulations: Experimental Design and Climate Models

4.1. Experimental Design

[28] The simulations consisted of 3-member ensemble transient climate simulations from 2000–2050 to isolate the effects of projected changes in the short-lived species and to calculate their importance relative to the long-lived GHGs. The use of an ensemble, meaning multiple simulations differing only in their initial conditions, reduces the unforced variability in the chaotic climate system. One set of runs included the evolution of short-lived and long-lived species following the A1B scenario, while the second set included only the evolution of long-lived species. In practice, NCAR performed only a single pair of simulations, while GISS and GFDL performed all three pairs for an

Table 4. Ratio of Sulfate and Ozone Burdens to Precursor Emissions, Global Mean Annual Average[a]

Species	Model	2000 Tg Burden/ Tg Emission	2030 Versus 2000 Tg Burden/ Tg Emission	2030 Versus 2000 % Burden/ % Emission	2050 Versus 2000 Tg Burden/ Tg Emission	2050 Versus 2000 % Burden/ % Emission
Sulfate	GFDL	.017	.017	1.00	.001[b]	0.08[b]
Sulfate	GISS	.012	.007	0.60	.007	0.65
Ozone	GFDL	9.2	2.8	0.32	4.0	0.44
Ozone	GISS	6.8	6.5	0.94	6.5	0.96

[a]Sulfate changes are Tg sulfate produced per Tg S in SO_2 emitted. Ozone changes are Tg ozone per Tg N in NO_x emitted. Ozone values in Table 2 in are converted to burden assuming 1 DU globally averaged = 10.9 Tg ozone.
[b]The burden change was o in this case, making the ratio less reliable.

Table 5. Aerosol Optical Depth (550 nm Extinction)–ALL-SKY

Region	Aerosol type	Model	2000	2030	2050
Global	BC	GFDL	.0076	.0096	.0105
		GISS	.0045	.0034	.0028
	sulfate	GFDL	.1018	.1227	.0906
		GISS	.0250	.0312	.0278
		NCAR	.048	.062	.052
	sea-salt	GFDL	.0236	.0236	.0236
		GISS	.1065	.1065	.1065
		NCAR	.0176	.0176	.0176
	dust	GFDL	.0281	.0281	.0281
		GISS	.0372	.0372	.0372
		NCAR	.0275	.0275	.0275
	OC	GFDL	.0104	.0122	.0131
		GISS	.0166	.0135	.0130
	nitrate	GISS	.0054	.0057	.0060
	total	GFDL	.1715	.1964	.1660
		GISS	.1952	.1975	.1933
		NCAR	.116	.1392	.1206
NH	BC	GFDL	.0109	.0147	.0161
		GISS	.0062	.0043	.0032
	sulfate	GFDL	.1509	.1766	.1038
		GISS	.0352	.0449	.0388
		NCAR	.065	.084	.060
	dust	GFDL	.0491	.0491	.0491
		GISS	.0600	.0600	.0600
	sea-salt	GFDL	.0181	.0181	.0181
		GISS	.0630	.0630	.0630
		NCAR	.0128	.0128	.0128
	total	GFDL	.2430	.2756	.2056
		GISS	.1910	.1954	.1875
		NCAR	.1538	.1827	.1502
SH	BC	GFDL	.0042	.0046	.0049
		GISS	.0029	.0026	.0023
	sulfate	GFDL	.0526	.0689	.0774
		GISS	.0148	.0175	.0170
		NCAR	.030	.040	.063
	dust	GFDL	.0071	.0071	.0071
		GISS	.0144	.0144	.0144
	sea-salt	GFDL	.0291	.0291	.0291
		GISS	.1502	.1502	.1502
		NCAR	.0224	.0224	.0224
	total	GFDL	.1000	.1171	.1263
		GISS	.1995	.1998	.1996
		NCAR	.0779	.0957	.0910

ensemble (with GFDL extending all three out to 2100, as discussed by *Levy et al.* [2008]).

[29] For the short-lived species, concentrations were taken from the prior composition simulations described above, with values for intermediate years linearly interpolated between the values for computed years. The one exception to this were stratospheric ozone changes. While these were calculated in a full chemistry model at GISS (allowing response to changing greenhouse gas abundances at all latitudes as well as recovery from halogen-induced depletion) as for short-lived species in the troposphere, a polar ozone recovery was prescribed linearly from 2010–2050 at GFDL, and stratospheric ozone in the NCAR model followed a prior simulation of the 21st century polar recovery due to reductions in CFCs [*Kiehl et al.*, 1999]. Hence polar springtime ozone recovery was qualitatively similar in the three models, but the increases that occur elsewhere in the GISS model [*Shindell et al.*, 2007] were not present in the other two.

[30] We remind the reader that the GFDL and NCAR simulations that include the time evolution of both short-lived and long-lived s are the simulations those groups performed for their IPCC AR4 A1B projections (though the IPCC projections were single runs rather than ensembles). The GISS simulation with time evolution of long-lived species only is nearly identical to that center's IPCC AR4 A1B simulation, differing only in the values of the fixed present-day aerosol and ozone distributions.

4.2. Climate Models

4.2.1. NOAA Geophysical Fluid Dynamics Laboratory

[31] Climate simulations at GFDL used the coupled climate model (AOGCM) recently developed at this center, (CM2.1), which has been previously described in detail [*Delworth et al.*, 2006]. The model simulates atmospheric and oceanic climate and variability from the diurnal timescale through multicentury climate change without employing flux adjustment. The resolution of the land and atmospheric components is 2.5° longitude × 2° latitude and the atmospheric model has 24 vertical levels. The ocean resolution is 1° in latitude and longitude, with meridional resolution equatorward of 30° becoming progressively finer, such that the meridional resolution is 1/3° at the Equator. There are 50 vertical levels in the ocean, with 22 evenly spaced levels within the top 220 m. The ocean component has poles over North America and Eurasia to avoid polar filtering. The model includes the radiative effects of well-mixed gases and ozone on the climate, as well as the direct effects of aerosols, but does not include indirect aerosol effects.

[32] The control simulation has a stable, realistic climate when integrated over multiple centuries, a realistic ENSO, reduced sea-ice biases in the North Atlantic compared to previous model versions and is able to simulate the main features of the observed warming of the 20th century. Its equilibrium climate sensitivity to doubled CO_2 is 3.4°C.

4.2.2. NASA Goddard Institute for Space Studies

[33] The climate simulations, like the composition simulations, were performed using GISS ModelE [*Schmidt et al.*, 2006]. We use a 20-layer version of the atmospheric model (up to 0.1 hPa) with 4° × 5° horizontal resolution coupled to a dynamic ocean without flux adjustment also run at 4° × 5° horizontal resolution, as in the GISS-ER IPCC AR4 simulations [*Hansen et al.*, 2007]. This model has been extensively evaluated against observations [*Schmidt et al.*, 2006], and has a climate sensitivity in accord with values inferred from paleoclimate data and similar to that of mainstream general circulation models (GCMs); it has an equilibrium climate sensitivity of 2.6°C for doubled CO_2.

[34] The modeled radiatively active species influence the climate in the GCM. Ozone and aerosols can affect both the short and long wavelength radiation flux. Water uptake on aerosol surfaces influences the aerosol effective radius, refractive index and extinction efficiency as a function of wavelength and the local relative humidity [*Koch et al.*, 2007], which in turn affects the GCM's radiation field.

[35] The GISS model also includes a simple parameterization for the aerosol indirect effect [*Menon et al.*, 2002]. This includes cloud cover changes following the empirical logarithmic dependence on the number concentration of soluble aerosols of *Gultepe and Isaac* [1999], where the number concentrations are determined from the aerosol masses based on densities and solubilities prescribed for each species as in *Hansen et al.* [2005]. Carbonaceous

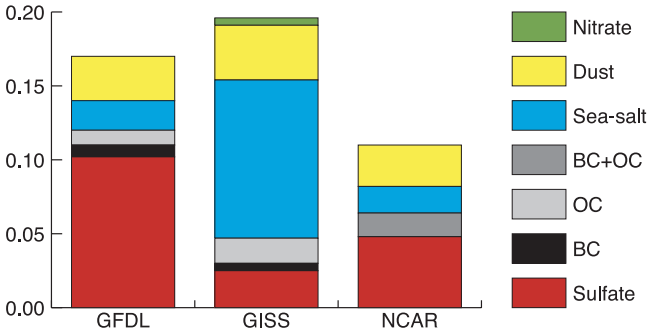

Figure 2. Present-day contributions from individual aerosol species to global mean all-sky aerosol optical depth (550 nm extinction). Neither GFDL or NCAR include nitrate.

aerosols become soluble after aging in the model, so the aerosol indirect effect depends upon BC, OC, sulfate and nitrate. In these simulations, we use only cloud cover changes (the 2nd indirect effect), with empirical coefficients selected to give roughly -1 W/m^2 forcing from the preindustrial to the present, a value chosen to match diurnal temperature and satellite polarization measurements, as described by *Hansen et al.* [2005]. We note, however, that this forcing is roughly twice the value of many other model studies [*Penner et al.*, 2006]. The aerosol indirect effect takes place only from the surface through ~630 hPa, as aerosols only affect liquid-phase stratus clouds in the model.

4.2.3. National Center for Atmospheric Research

[36] The transient climate simulations use the NCAR CCSM3 [*Collins et al.*, 2006]. This model had been run previously with evolution of short-lived species in the future for the IPCC AR4. The model was run at T85 (~1.4° × 1.4° resolution) in the atmosphere with a vertical resolution of 26 levels from the surface to 4 hPa. Horizontal resolution in the ocean was 1° × 1°. For this study, a new simulation was performed for 2000–2050 in which ozone and aerosols were kept at their 2000 levels. The equilibrium climate sensitivity of this model to doubled CO_2 is 2.7°C.

[37] Aerosol optical properties are affected by the local relative humidity distribution, which then affects the radiative heating calculation and the climate simulations. In these model runs, there is no representation of the aerosol indirect effect.

5. Climate Results

5.1. Radiative Forcing

[38] The instantaneous radiative forcing at the tropopause provides a useful, though limited, indicator of the climate response to perturbations [*Hansen et al.*, 2005] (NCAR did not calculate RF). The net global mean annual average RF from short-lived species at 2030 relative to 2000 is small in both the GFDL and GISS models (Figure 3 and Table 6). In the GFDL model, a large increase in sulfate optical depth leads to a negative forcing that is largely balanced by positive forcings from increased BC and ozone. In contrast, in the GISS model, increased sulfate and reduced BC both lead to relatively small negative forcings that largely offset a substantial positive forcing from increased ozone. By 2050 the models diverge i r net values as well as the contributions from individual species. GFDL finds a large positive net forcing due in nearly equal parts to increased BC and ozone. In contrast, 2050 net forcing in the GISS model again reflects an offset between positive forcing from ozone and negative aerosol forcing, with the largest contribution to the latter being reduced BC. The models both show a cancellation of a small portion of the BC forcing by an opposing forcing from OC.

[39] Intermodel differences in RF are predominantly due to the changes in modeled burden rather than to differences in the calculation of radiative properties in the models. This can be seen clearly by examining the RF-to-burden ratio, which we term the radiative efficiency (Table 7). The radiative efficiencies are fairly similar for GFDL and GISS. The largest differences are seen for BC, which may reflect differences in the geographic location of projected BC changes as well as differing treatments of BC's radiative properties. Additionally, the vertical distribution of the BC changes will affect the RF, as will their location relative to clouds. Variations in modeling the aerosol uptake of water, which can have a substantial impact on the AOD, do not seem to play a very large role in the global mean RF judging from the fairly close agreement in the two models' sulfate radiative efficiencies (Table 8). Examination of the RF-to-AOD change (Table 8) shows that given a particular AOD change, the models are in good agreement as to the resulting radiative forcing. This contrasts with the results of a wider study of models [*Schulz et al.*, 2006], suggesting a possible further source of model differences that could exist were different models to be used in a study such as this.

[40] Both the GFDL and GISS models show a positive forcing from ozone that stems partially from increased tropospheric ozone pollution due to increased NO_x emissions (Table 1) and partially from the recovery of stratospheric ozone. The forcing from the tropospheric ozone changes is substantially more important, however [*Shindell et al.*, 2007]. While the NCAR group did not calculate radiative forcings, their RF from ozone is likely to have been similar to those of GFDL and GISS, as their tropospheric ozone burden increase was very close to the GISS value (Table 2). Given the large differences between the GFDL and GISS ozone projections discussed previously, the similarity in the RF in these models is largely fortuitous.

[41] Hence overall at 2030, differences in the physical processes in the two models are important. The large divergence in RF from sulfate stems from both the chemical conversion efficiency of SO_2 to sulfate being more than a factor of two larger in the GFDL model than in the GISS model, and the relatively greater role of sulfate in AOD in the GFDL model. This is at least partially due to the inclusion of substantial absorption of sulfate onto dust in the GISS model, a process that is highly uncertain. At 2050, emissions of sulfur dioxide have returned to near their 2000 level, so that these physical differences are not so important at this time. Instead, the 2050 aerosol differences between the two models are dominated by differences in BC emissions projections. Differences in the BC production and radiative efficiencies in the two models are substantial, but offset one another.

[42] On a hemispheric scale, the GISS and GFDL models again differ greatly (Table 8). At 2050, GFDL shows a very large positive NH forcing from sulfate and BC, and a

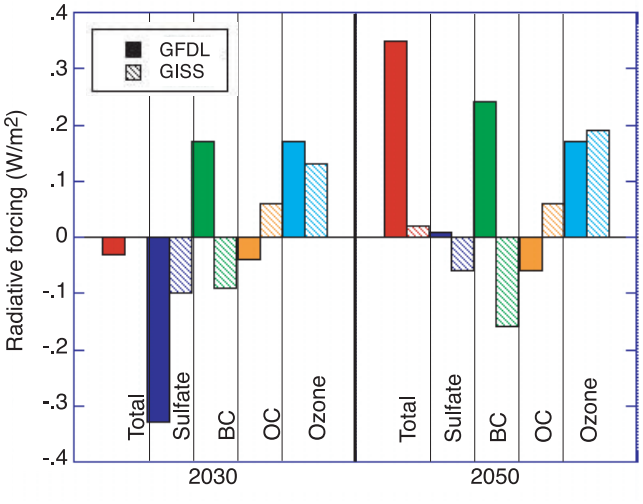

Figure 3. Global mean annual average radiative forcing from short-lived species at 2030 and 2050 relative to 2000. Values from the GFDL model are shown as solid bars, values from the GISS model have diagonal hatching.

negative SH forcing primarily from sulfate. In the GISS model, RF is negative in the NH due to the reduction in BC and positive, due to increased ozone and reduced OC, in the SH (where sea-salt dominates the AOD, so that anthropogenic aerosol emissions changes are relatively less important).

[43] Comparison of the spatial patterns of RF in the GISS and GFDL models reveals that the starkest discrepancies for aerosols occur near the developing nations of South and East Asia (Figure 4). The emissions scenario used by the GISS model projects strong increases in sulfate emissions from India, with little change over China. In contrast, the scenario used by the GFDL model has large decreases in sulfate emissions in both regions, especially China. In contrast, the sulfur scenarios are much more similar for the developed world. Differences are even larger for BC, which increases throughout most of the NH in the GFDL model but decreases in the GISS model. Again, the divergence is largest over South and East Asia (Figure 4). Thus the differences in the global total emissions (Figure 1 and Table 1) and in the global RF (Figure 2 and Table 6) arise primarily from differences in projected emissions from developing countries in Asia.

[44] The RF from OC is generally similar in its spatial pattern to that from BC, but of opposite sign and substantially reduced magnitude (25–40% of the BC RF). As discussed previously, the GFDL model assumed that biomass burning emissions were 50% anthropogenic and 50% natural (and thus would scale by $^1/_2$ the factor used for purely anthropogenic emissions). The GISS model instead used regional biomass burning emissions projections from *Streets et al.* [2004]. These consist of distinct trends in emissions from individual source types, and lead to substantial reductions in African vegetation biomass burning over time and relative to the GFDL scenario.

[45] The spatial pattern of RF from ozone is also substantially different in the two models (Figure 4). The forcing in the GISS model is not closely tied to the region of precursor emissions, but instead is related to an increased flux of ozone into the t here owing to the recovery of lower stratospheric ozone. At low latitudes, GISS shows little forcing as the modeled increase in upper stratospheric ozone causes negative RF and alters lower level photochemistry. Furthermore, the aerosol indirect effect in that model influences cloud cover and wet deposition, which seems to reduce tropospheric ozone at low latitudes in comparison with simulations not including the AIE. The GFDL model instead shows maximum ozone forcing in the tropics. This may reflect a greater geographic shift in emissions to lower latitudes, a greater efficiency in transporting ozone and its precursors to the upper troposphere, where ozone has the greatest positive forcing efficiency, or differences in the models' chemistry, as well as the influence of the stratosphere and AIE. Note that the GFDL simulations of tropospheric composition did not include future recovery of stratospheric ozone, and thus did not produce increased fluxes of ozone from the stratosphere into the troposphere.

5.2. Surface Temperature Response

[46] Though the models used different emissions and contained different physical processes, the global mean annual average temperature responses to short-lived species are not as dissimilar as one might have expected. The NCAR simulation showed little or no statistically significant effects of the short-lived species on global mean surface temperatures (though there is a suggestion that short-lived species induce cooling of ~0.1 K near the end of the run). The GFDL and GISS models both show a statistically significant warming effect from short-lived species from around 2030 to the end of the runs (Figure 5). The GFDL model shows a warming of 0.28 K (ensemble mean 2046–2050). This value is roughly commensurate with a climate forcing of 0.3 W/m^2 and that model's climate sensitivity (~0.8°C per W/m^2) [*Levy et al.*, 2008]. The GISS model shows a mean 2046–2050 warming of 0.13 K, substantially more than would be expected from the direct radiative forcing in that model and its climate sensitivity (~0.6°C per W/m^2). This appears to be due principally to the AIE, which contributes additional warming as aerosol loading decreases in the future [*Shindell et al.*, 2007]. Note that the GISS and NCAR models have relatively similar variability (NCAR variability appears larger as there was only 1 NCAR simulation while the other models had 3), but the GFDL model's variability is substantially larger. This is presumably related primarily to differences in the ocean models. We note also that the response does not necessarily follow the forcing as closely for spatially inhomogeneous forcings as it does for homogeneous forcings, since even a zero global mean forcing can lead to a non-zero global mean response [*Berntsen et al.*, 2005].

[47] The overall influence of short-lived species on global annual average temperatures is to augment the warming from well-mixed GHGs by ~20–25% in these two models (17% for GISS and 27% for GFDL based on 2046–2050 versus the first 5 years of the run). It is important to note, however, that these models responded as they did for different reasons. In the GFDL simulations, reduced sulfate and increased BC and ozone all combined to cause warming. In contrast, in the GISS model, the warming resulted from increased ozone and a reduced AIE, with a substantial offset of these from reduced BC. The lack of a substantial

Table 6. Global Radiative Forcing (W/m^2)[a]

	Model	2030	2050	2100
Total	GFDL	−0.03	0.37	0.97
	GISS	0.00	0.02	NA
Aerosols	GFDL	−0.20	0.19	0.85
	GISS	−0.13	−0.17	NA
Sulfate	GFDL	−0.33	0.01	0.51
	GISS	−0.10	−0.06	NA
BC	GFDL	0.17	0.24	0.51
	GISS	−0.09	−0.16	NA
OC	GFDL	−0.04	−0.06	−0.15
	GISS	0.06	0.06	NA
Ozone	GFDL	0.17	0.17	0.12
	GISS	0.13	0.19	NA

[a]Values are annual average instantaneous forcings at the tropopause (meteorological tropopause in GISS GCM, "linear" tropopause in GFDL GCM). "Aerosols" is simply the total of sulfate, BC, and OC (plus nitrate for GISS). GISS values do not include aerosol indirect effects that were present in that model.

effect from short-lived species in the NCAR simulations is attributable to their emission trajectories, which had small increases in sulfate (cooling) and small increases in BC (warming) that largely offset one another (their AOD changed little from 2000 to 2050).

[48] The response to well-mixed GHGs is also different among the models, and does not simply follow the climate sensitivity of the GCMs. The long-lived species induce substantially greater warming in the NCAR model although that model has an equilibrium climate sensitivity to doubled CO_2 (2.7 C) almost the same as the GISS model's (2.6 C) and significantly less then the GFDL model's (3.4 C). Factors that could account for the variations are differences in the halocarbon species included, in the models' radiation codes, and in the experimental setup. In the GISS GCM, for example, short-lived species from an earlier model version were used for the 20th century, with fields from the newer model used for the 21st. This led to an instantaneous increase in aerosol cooling at 2000. While this was removed from the calculation of the effect of short-lived species by differencing the long-lived+short-lived species with the long-lived species only runs, it reduced the response in both runs and hence decreases the warming due to long-lived species alone shown here. Additionally, it may be that the transient climate sensitivity is not as closely correlated with the equilibrium sensitivity as one might suppose.

[49] Hemispheric temperatures show trends largely consistent with the radiative forcings (Table 7), namely substantial warming by 2050 in the NH in the GFDL model and in the SH in the GISS model (Figure 6).The NH warming in the GFDL model is driven primarily by the large decreases projected for sulfate and large increases projected for BC in that model for North America, Europe and especially South and East Asia [*Levy et al.*, 2008]. This causes the AOD from sulfate to drop by 1/3 in the NH by 2050 while the AOD from BC increases by 50%. The large change in sulfate dominates the overall AOD change in that model (Table 5). The magnitude of the NH warming is ~0.5 K by 2050, consistent with the 0.9 W/m^2 radiative forcing in that model accounting for the fact that the warming has not been fully realized due to the lag-time for oceanic heat adjustment (the equilibrium response would be 0.9 $W/m^2 \times 0.8°C$ per $W/m^2 = 0.7$ K). There is an overall negative forcing in the SH in the GFDL model, as sulfate precursor emissions increase in Africa and Latin America, while BC changes little. Some of the negative forcing from aerosols in the SH is offset by positive forcing from ozone, which increases over much of the developing world in that model [*Levy et al.*, 2008], leading to a small net effect and minimal temperature change from short-lived species (Figure 6). There is some SH warming after about 2030 however, suggesting that the SH may be feeling the effects of the large positive NH forcing more strongly than the smaller negative SH forcing (Table 7).

[50] The AIE in the GISS model was argued to be on the order of 0.1–0.2 W/m^2 in the 2030–2050 time period [*Shindell et al.*, 2007], which would make the net NH forcing zero to slightly positive and would increase the SH forcing to ~0.3–0.4 W/m^2. These forcings are consistent with the warming of ~0.15 K seen in that model in the SH and the small (~0.07 K) response in the NH. The signs of the direct RF in the two hemispheres are opposite in the GISS model to what they are in the GFDL model (Table 7). This is because in the GISS model, NH aerosol changes are dominated by a substantial reduction in BC (the NH BC AOD falls by nearly 50%), which more than offsets a slight increase in sulfate (particularly as this model is less sensitive to sulfate). Thus the aerosol changes lead to negative NH forcing, opposite the GFDL positive forcing driven by decreases in sulfate and increases in BC. In the SH, the GISS model shows only small changes in aerosols, so that positive forcing from ozone dominates the net RF. This is again opposite the GFDL model, which has a negative radiative forcing primarily from sulfate. In the GISS model, the AIE further accentuates the SH positive forcing owing to reductions in BC and OC.

[51] As for the global case, hemispheric temperature trends in the NCAR model are not significantly different in the runs with and without short-lived species. This is the result of only a miniscule change in AOD in the NH (−2%), as sulfate and carbonaceous aerosol loadings are both near their present-day values by 2050 in that model. This leads to a small NH cooling (also visible in the global mean, Figure 5), but it is not significant at the 95% confidence level. In the SH, there is an increase in AOD from 2000 to 2050 in the NCAR model, which seems to be largely due to sulfate, but this is opposed by increased ozone in the SH as stratospheric ozone recovers.

[52] Thus it is clear that at global and especially at hemispheric scales, the three climate models are being driven by substantially different trends in their aerosol

Table 7. Radiative Efficiency[a]

Species	Model	$(W\ m^{-2})/Tg$	$(W\ m^{-2})/AOD$
BC	GFDL	2.2	83
	GISS	1.5	94
OC	GFDL	−0.18	NA
	GISS	−0.16	NA
SO_4	GFDL	−0.48	−16
	GISS	−0.59	−16

[a]Values are given for the radiative efficiency in terms of the RF-to-burden ratio and the RF-to-AOD ratio. All values are global mean annual averages. Values for RF and burden or AOD changes are from 2050 versus 2000 for BC and OC, and 2030 versus 2000 for sulfate in order to analyze the largest changes for each species. GISS values for the sulfate burden changes include only the portion of sulfate not absorbed onto dust, as this portion alone is radiatively important.

Table 8. Hemispheric Radiative Forcing (W/m^2)[a]

	Model	2030	2050	2100
NH	GFDL	0.07	0.96	1.66
	GISS	−0.15	−0.14	NA
SH	GFDL	−0.13	−0.25	0.27
	GISS	0.16	0.18	NA

[a]Values are annual average instantaneous forcings at the tropopause. GISS values do not include aerosol indirect effects that were present in that model.

species. These differences in aerosols are largely related to the differences in the projected emissions of aerosol precursors, though there is some contribution from differences in modeling of aerosol physics as discussed previously. Additionally, the climate response is different to some extent owing to the inclusion of different physical processes in the models, especially having the AIE in the GISS model. However, the above analysis strongly suggests that the largest contributor to the intermodel variations in projected surface temperatures is the differing assumptions about aerosol precursor emissions trends.

[53] Examining smaller spatial scales, the patterns of surface temperature changes induced by the short-lived species show even larger divergences among the models (Figure 7). Around 2030, the largest responses are seen at Northern middle and high latitudes. These show large regions of both cooling and warming that are characteristic of the response to dynamic variations, especially during the colder half of the year. Surprisingly, all three models show cooling near Alaska and a region of warming over Siberia. However, most of the temperature response at these latitudes is not statistically significant in the models owing to large natural variability during the extended winter. Other regions, such as the Labrador Sea/Baffin Island area or Scandinavia, show substantial variations between models, again suggesting these NH middle and high latitude dynamic responses are not robust.

[54] In the tropics, where dynamic variability is much smaller, the models find much greater areas with statistically significant responses, especially by 2050. The NCAR model finds a small but significant cooling over tropical oceans, while the other two models find warming. This appears to again result from intermodel differences in aerosols. In the NCAR model, the cooling results from increased sulfate, while in the GFDL model the warming is primarily due to decreased sulfate and increased BC (Table 5). In the GISS model, the aerosols lead to warming due in part to the reduction of the AIE. Hence the differences in simulated temperatures are due to differing aerosol emissions projections and aerosol physics in the models.

[55] Over the Antarctic, the GISS model shows warming related in part to stratospheric ozone recovery. The GFDL model shows a similar result by 2050. NCAR does not show Antarctic warming, however, even though this model also included recovery of ozone in the Antarctic lower stratosphere. This lack of an Antarctic warming is surprising given that the NCAR model appeared to show a substantial response to ozone depletion in analyses of the SH circulation in IPCC AR4 simulations [*Miller et al.*, 2006b]. This analysis showed that most climate models found a general strengthening of the westerly flow in the SH in response to stratospheric ozone depletion. A stronger flow isolates the polar region from lower latitude air, leading to cooling over the Antarctic interior and warming at the peninsula. Conversely, recovery should lead to warming of the interior (enhanced by the direct positive RF from increased ozone), as in the GISS and GFDL simulations. However, even in those models the effect does not simply increase with time (as ozone amounts do), suggesting that other aspects of the response to short-lived species also play a role in the Antarctic temperature response.

[56] Warming over the central US is present in the GISS model at all times (but is not statistically significant), in the GFDL model from about the 2040s on, and in the NCAR model around 2030, but not at 2050. The US and other NH industrialized regions may be especially sensitive due to the projected reduction in sulfate precursor emissions in those areas. This effect is especially large in the GFDL model, where sulfate decreases and BC increases, both contributing positive forcings. In the NCAR model, the effect vanishes by 2050 as both sulfate and BC decrease, canceling one another. In the GISS model, reductions in sulfate and increases in ozone both contribute positive forcings, though these are partially offset by reduced BC.

[57] Overall, it is clear that the regional response does not closely follow the regional RF based on either GISS or GFDL results. Both models show very large forcings over South and East Asia, for example, yet have minimal response there. Additionally, the GFDL model shows warming over Africa and South America despite negative net RF there. As shown in *Shindell et al.* [2007], the mismatch between the spatial patterns of RF and climate response in the GISS model cannot be accounted for by the AIE. Consistent with these results, earlier studies have found similar discrepancies between forcing and response patterns in the cases they examined [*Mitchell et al.*, 1995; *Boer and Yu*, 2003; *Berntsen et al.*, 2005; *Hansen et al.*, 2005].

5.3. Precipitation Response

[58] Changes in other climate parameters such as precipitation or sea level due to short-lived species are typically too small to isolate statistically. These would be expected to generally follow the global mean surface temperature change, however, for many of the most important features. For example, the portion of sea level rise attributable to thermal expansion of the oceans would ultimately be enhanced by ~20–25% due to short-lived species under the GISS and GFDL models. Similarly, the enhancement of precipitation along the equator and drying of the subtropics that is a robust feature of GCMs under a warming climate [*Held and Soden*, 2006] would also be accentuated under the GFDL and GISS models with their significant tropical warming, though probably not under the NCAR scenario. Such a feature can indeed be seen in the GISS precipitation response in the Atlantic and Indian Oceans (not shown).

[59] On a regional scale, there are some suggestions of trends in precipitation but statistical significance is marginal. The NCAR model shows reductions in winter precipitation due to short-lived species across most of the US in the 2040s, and reductions in summer precipitation in the SE US. That model also suggests an increase in summer monsoon rainfall over South Asia. In contrast, the GISS

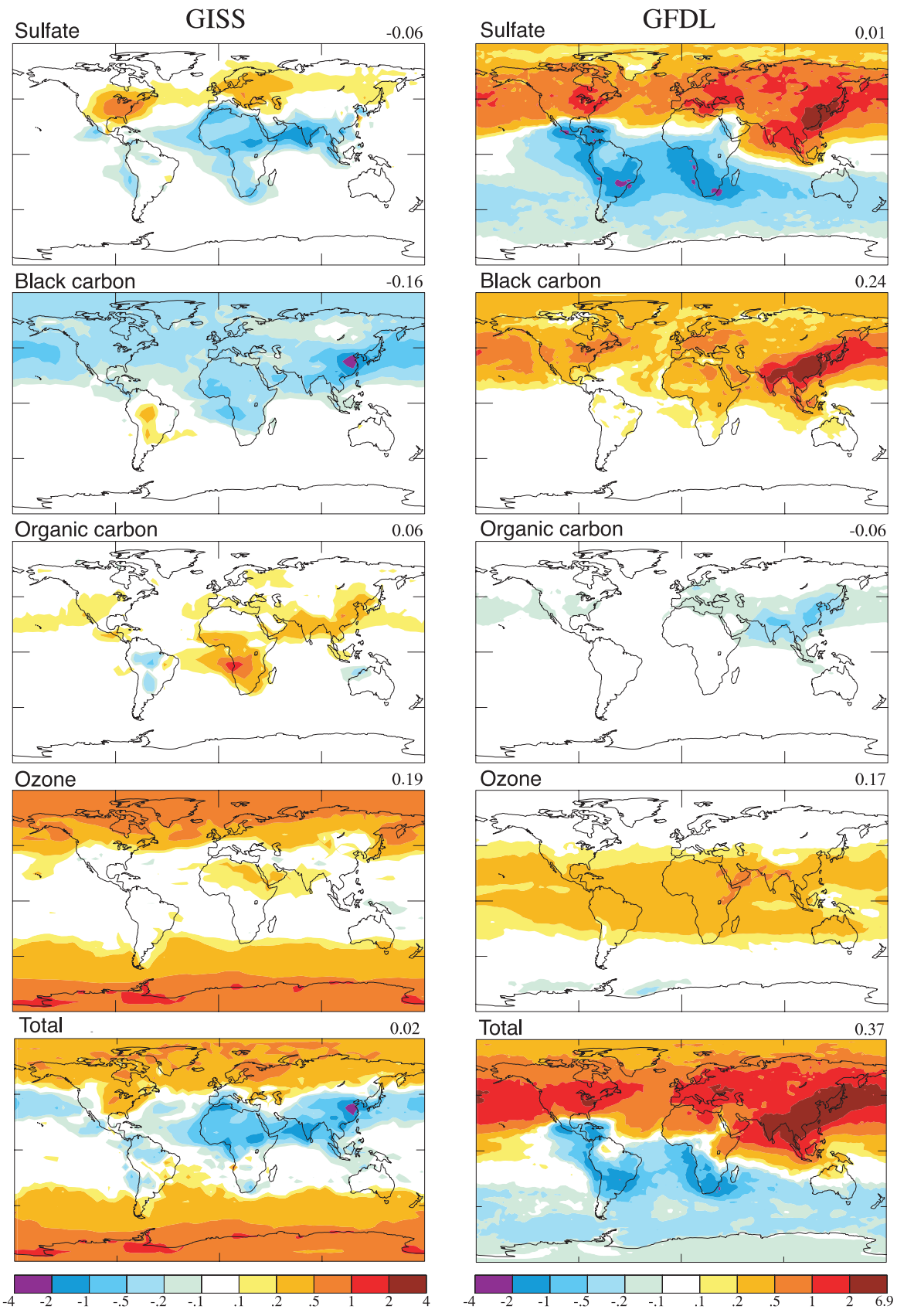

Figure 4. Annual average instantaneous radiative forcing (W/m^2) at the tropopause near 2050 relative to 2000 for the indicated individual short-lived species in the GISS (left) and GFDL (right) models and their totals (bottom row). Values in the upper right corner of each panel give the global mean.

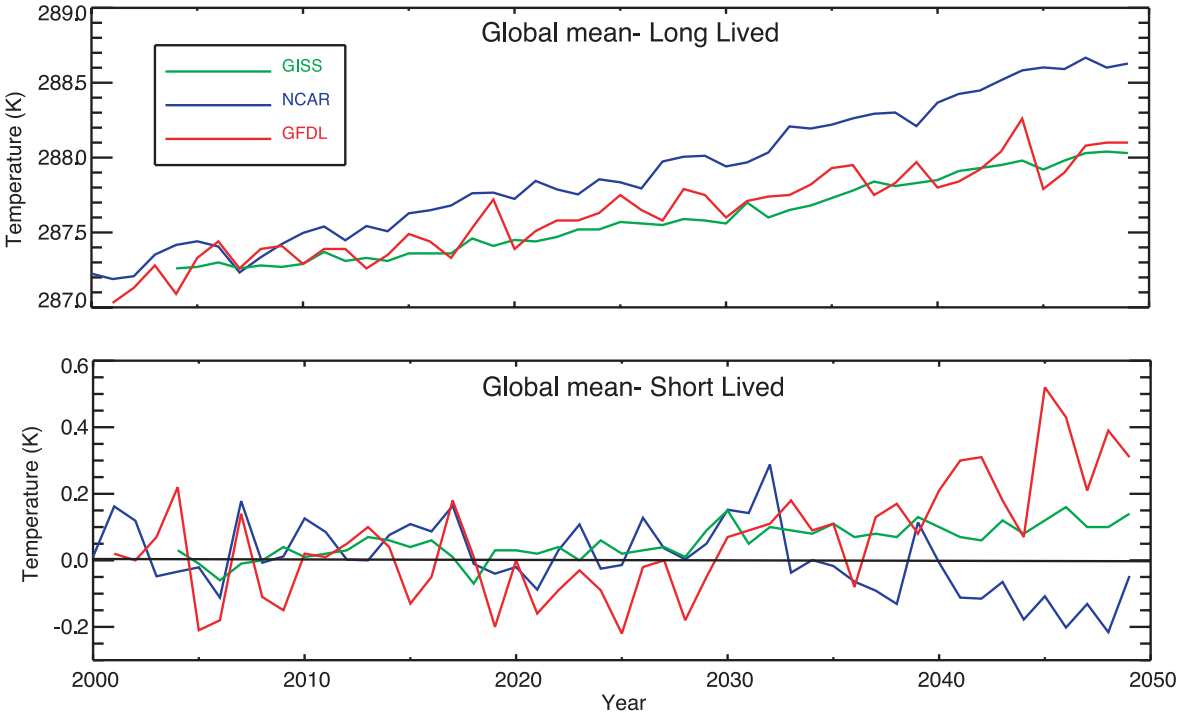

Figure 5. Global mean annual average temperature in the simulations with time-varying long-lived species only (top) and due to short-lived species based on the ((long-lived+short-lived)-long-lived) difference (bottom). Results are ensemble means for GFDL and GISS.

model shows slight increases in winter precipitation over the central US, and a mixed signal in summer (and spring) with increased precipitation over the SE and SW but decreases over the NE. During fall, precipitation decreases over most of the country. As in the NCAR model, there is an increase in summer (and fall) precipitation over South Asia. Looking at the annual average, the GFDL model shows no statistically significant trend over the US. Given that significant trends are hard to identify in any of the models, and that the models do not agree on the trends themselves, we believe that it is not possible to reliably estimate precipitation trends owing to short-lived species changes under the A1B storyline.

5.4. Discussion

[60] In the transient climate simulations, three climate models examined the response to projected changes in short-lived species. The results differed substantially among the models. Comparison has shown that the differences in the underlying emissions projections, due to differences between the various IAMs that provided those projections and to assumptions made about emissions not provided by the IAMs, were the dominant source of intermodel differences in projected aerosol trends. These were not the only source of differences, however. For example, sulfate plays a much larger role in the GFDL model's AOD than the GISS model's, with the NCAR model in between. This is partially due to the inclusion of sulfate absorption onto dust only being present in the GISS model. Additionally, the indirect effect of aerosols was only included in the GISS model. Thus the inclusion of different physical processes played a role in the intermodel differences, and was especially important near 2030 w O_2 emissions were near their peak. With the inclusion of the AIE, the GFDL model might yield a substantially larger warming given that sulfate is the largest contributor to aerosol mass globally and their sulfate decreased in the future.

[61] Intermodel differences were also created by the models' differing simulations of the hydrologic cycle, which removes soluble species, and of oxidation. Intermodel differences between the GFDL and GISS models in the conversion efficiency of SO_2 to sulfate aerosol were substantial, and differences in the radiative effect of BC were also potentially sizable. In many cases, however, these were outweighed by emissions differences. This was not the case for sulfate at 2030, nor for tropospheric ozone, for which differences in sensitivity of ozone to NO_x emissions (which may indirectly reflect differences in stratospheric ozone projections as well as tropospheric differences) were larger than differences in projected precursor emissions, and thus uncertainties in physical sciences appear to dominate over uncertainties in socio-economics.

[62] The results clearly indicate that the spatial distribution of radiative forcing is less important than the spatial distribution of climate sensitivity in predicting climate impact. It is worth noting that metrics other than RF, at least in some regions, might be better predictors of climate response, however. For example, snow and ice covered regions may be more sensitive to surface radiative fluxes rather than to tropopause or top-of-the-atmosphere forcing. Additionally, localized RF may have different effects at either much shorter or much longer timescales than those explored here (e.g., on weather, or on the long-term response of the coupled land-atmosphere system). For multidecadal timescales, however, both short-lived and long-lived species

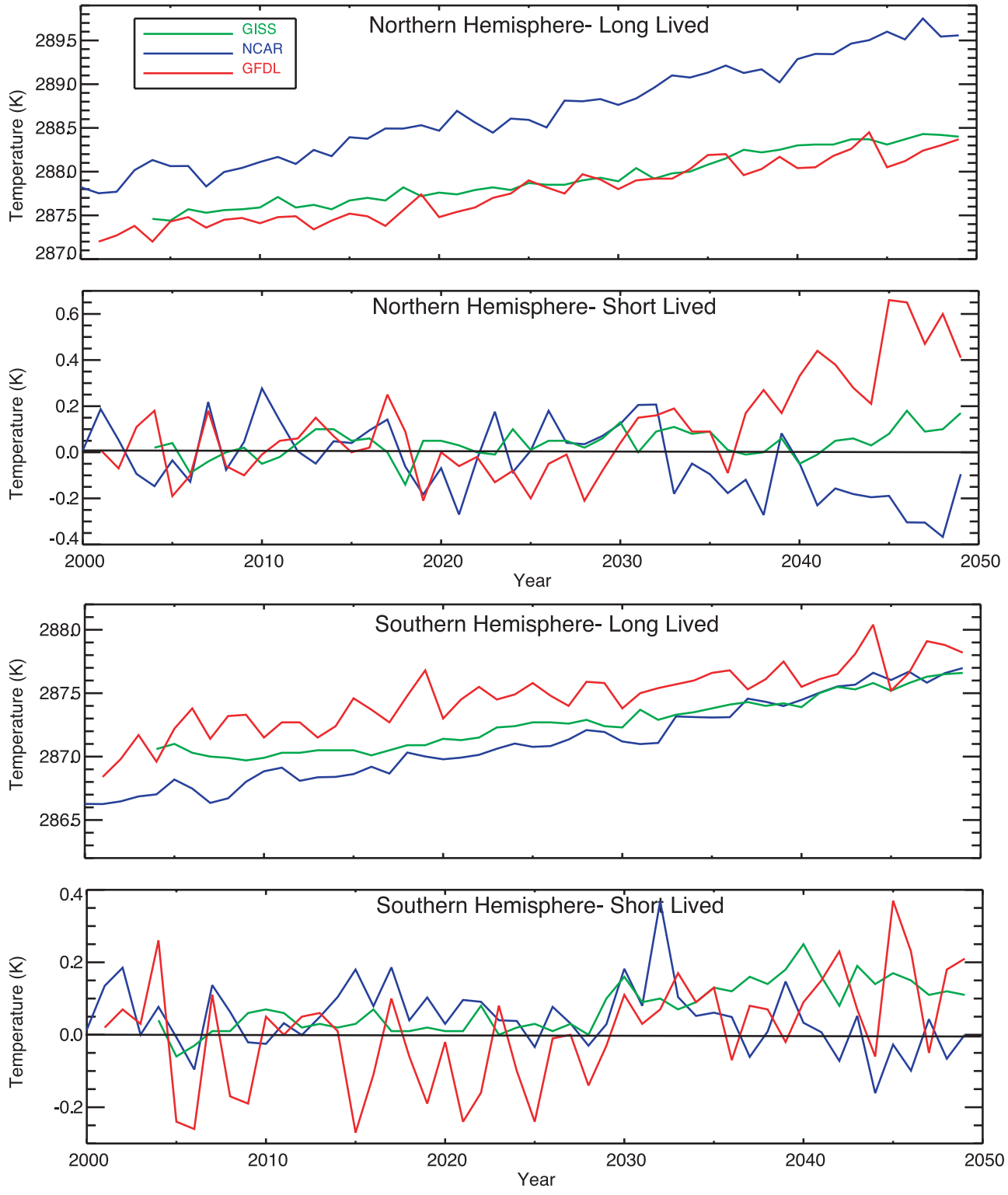

Figure 6. Hemispheric mean annual average temperature in the simulations with time-varying long-lived species only (first and third panels) and due to short-lived species based on the ((long-lived + short-lived)-long-lived) difference (second and fourth panels). Results are ensemble means for GFDL and GISS.

appear to cause enhanced climate responses in the same regions of high sensitivity rather than short-lived species having an enhanced effect primarily in or near polluted areas. This result is supported by analysis of the response to larger radiative perturbations in these models for the future [*Levy et al.*, 2008] and the past [*Shindell et al.*, 2007]. This suggests that the mismatch between model simulations of the regional patterns of 20th century

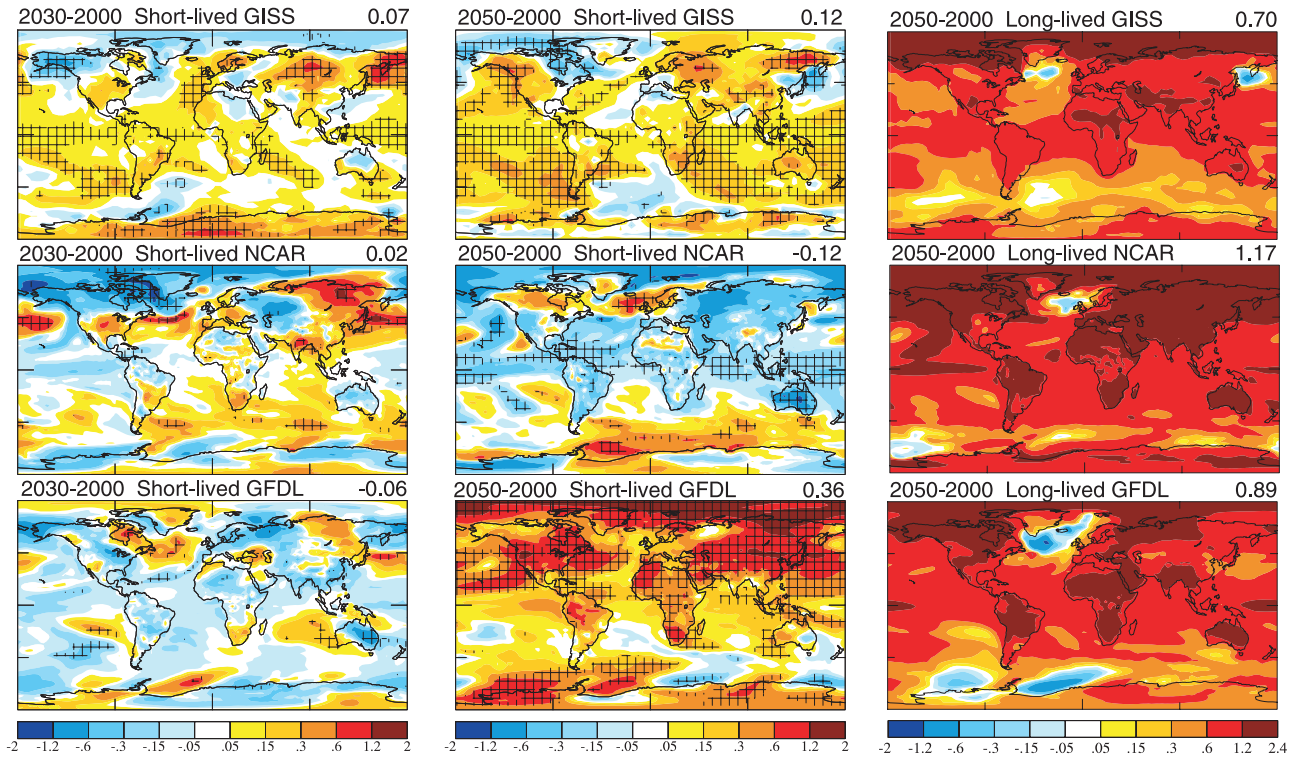

Figure 7. Annual average surface temperature change in the climate models due to short-lived species changes for the indicated times (left and center) and due to long-lived species (right). The changes at 2030 are 2020–2029 in the NCAR and GFDL models and 2028–2033 in the GISS model. At 2050, they are 2040–2049 in the NCAR model, 2046–2055 in the GFDL model, and 2040–2050 in the GISS model. Hatching indicates 95% statistical significance in the response to short-lived species, while all colored areas in the response to long-lived species are significant.

climate trends and observations is likely not attributable to unrealistic spatially inhomogeneous forcings imposed in those models. Instead, the models may exhibit regional climate sensitivities that do not match the real world, and/or some of the observed regional changes may have been unforced.

6. Conclusions

6.1. Emissions Projections

[63] The analysis presented here showed that the main contributors to the divergence among model projections of future aerosol loading and climate forcing were the differences in the underlying emissions projections. Those differences arose because: (1) different IAMs interpret a common socio-economic "storyline" in different ways, and (2) some short-lived species were not projected by the IAMs and had to be added in later by other emissions modeling groups or by the climate modeling groups themselves. Additionally, the global chemical transport models all used their own natural emissions. Though these were constant, they influence the response to perturbations by determining the background abundance of short-lived species. As the production efficiency, e.g., for ozone, is non-linear, different present-day emissions will affect the projections for the future.

[64] As the greatest divergences in our study came from the carbonaceous aerosols that were not projected by the IAMs, we strongly recommend that future IAM emission scenarios pay greater attention to the short-lived species and provide consistent emissions projections for carbonaceous aerosols and ammonia along with the other short-lived and long-lived species. We are aware that many IAMs are already capable of providing this information.

[65] We also recommend that climate models make greater efforts to study the effects of short-lived emissions projections in a manner that isolates their effect from that of the long-lived GHGs. In particular, we believe there is merit in continuing to use a broad distribution of IAM output to realistically characterize the range of potential futures for a given socio-economic storyline. In order to understand the contribution of uncertainties in the composition and climate models to this range, it would also be worthwhile to perform a controlled experiment with identical emissions projections using multiple chemical-transport and climate models.

[66] Finally, given our results that plausible scenarios for short-lived species can lead to a substantial climate response, it is important that model intercomparisons coordinate short-lived species projections. Current intercomparisons such as the AR4 include models with various treatments of short-lived species in the future (e.g., time-evolving for some species with globally uniform scaling, time- and space-evolving for some species, no changes), so that the contribution of differences in models' climate responses and in

climate forcing agents to the spread of model projections cannot be easily separated.

6.2. Physical Processes

[67] We also emphasize that several aspects of the modeling of physical processes have large uncertainties, especially for aerosols. This distinction is important, as uncertainties in physical processes can in principle be reduced through improved measurements of the climate system, while socio-economics has inherent irreducible uncertainties. Existing observations of aerosol optical depth are best able to constrain the total clear-sky optical depth of all aerosols, but not to identify the effect of individual species. Improved measurements of optical extinction and absorption may allow the reflective and absorbing classes of aerosols to be separated, but will not solve the fundamental problem of determining the relative importance of all the various species. As seen in this and other studies, models exhibit a wide range of relative contributions from the various natural and anthropogenic aerosols to the total. Thus the direct radiative effect of changes in a particular aerosol species can be substantially different among models depending upon the relative importance of that aerosol. So while the physics of an individual aerosol's direct effect is relatively well understood, there are still substantial uncertainties in its change with time. Furthermore, aerosol optical properties depend upon the particle size distribution, which is often prescribed or modeled rather crudely. Additionally, aerosol species mix together, a process that is only beginning to be incorporated in composition and climate models.

[68] Aerosol uptake of water vapor, which alters the size and optical properties of the aerosol, is now included in all mainstream climate models. As the uptake varies exponentially with relative humidity, small discrepancies in how this process in included in GCMs or in the distribution of humidity in the models have the potential to cause large differences. The results analyzed here, however, suggest that the differences induced by this process may be small relative to the others we have just discussed.

[69] The indirect effects of aerosols on clouds are very poorly known. Many aspects of aerosol-cloud interactions are not well quantified, and hence the effect was left out entirely in the GFDL and NCAR simulations. The GISS model used a highly parameterized approach that is quite crude. Given that the inclusion of the AIE played a substantial role in that model's response, it is clear that better characterization of these effects is imperative.

[70] It is also clear that some potential processes have not been included yet. An example is interactive dust loading, which can influence the composition of other short-lived species and can also be influenced by those species (e.g., via changes in solubility due to nitrate or sulfate uptake [*Fan et al.*, 2004; *Bauer and Koch*, 2005]). Other processes of potential importance that were not included in these transient climate simulations are changes in sea-salt and changes in darkening of snow and ice surfaces by BC deposition.

[71] Additional observations are clearly needed to better constrain the optical properties of aerosols. We recommend emphasis on long-term aerosol monitoring from ground and space, and on better cha zation of aerosol microphysics in the laboratory. To better characterize the processes governing the AIE, observations such as those taken from aircraft campaigns might be extremely useful. We also recommend greater use of the distinction between scattering and absorbing aerosols to characterize their relative importance.

[72] Uncertainties in physical processes exist in other areas as well. Two examples are the potential role of climate change in altering large-scale atmospheric circulation so as to affect stratosphere-troposphere exchange of ozone, and the potential response of methane emissions to climate change and the response of emissions of other hydrocarbons that influence methane's loss rate. Both these processes were show to have substantial potential impacts on future radiative forcing in [*Shindell et al.*, 2007], though both are highly uncertain. Finally, the effects of climate change in general on the short-lived species were not included as future compositions were simulated offline without including climate change.

6.3. Climate and Air Quality Policy Interdependence

[73] Most of the future sources of short-lived species result from the same combustion processes responsible for the increases in atmospheric CO_2. However, reductions in their emissions will be driven by local and regional air pollution issues that can be addressed independently of any reductions in CO_2 emissions, and climate responses can be felt more quickly than for CO_2 changes because of their shorter chemical lifetime. The good news is that there are win-win solutions for climate and air quality: methane, CO and VOC reductions [*Hansen et al.*, 2000; *Fiore et al.*, 2002; *Shindell et al.*, 2005; *West and Fiore*, 2005]. BC is a potential win-win as well. On the other hand, the reduction of sulfate or OC results in the loss of cooling and hence increased global warming.

[74] The cases of BC and NO_x are illustrative of the complexities of this issue. A major source of BC is biofuel combustion. Biofuel is CO_2 neutral (other than potential initial CO_2 responses due to land-use changes for new sources). Current suggested replacements result in the release of fossil CO_2. Therefore this reduction in BC will result in a net increase in CO_2. The actual net surface temperature response from substitution of fossil fuels for biofuels is not clear. The case of NO_x reductions appears to be approximately neutral for climate, though clearly highly beneficial for air quality. Reducing NO_x reduces ozone (in most areas), which reduces the global mean surface temperature, but reduced ozone and NO_x lead to less hydroxyl radical, a longer lifetime and therefore a greater abundance of methane, which increases the global mean surface temperature (and less nitrate, which also leads to warming). We must pay careful attention to the "Law of Unintended Consequences".

[75] Now to examine the problems we face in projecting future emissions for short-lived species. Future climates are only weakly dependent on the projected emissions of short-lived species for the next 20 years when, due to the inertia in the major emitters of most short-lived species, we may have credibility in forecasting emission trends for species such as sulfate or NO_x. However, we have shown that plausible emission scenarios for SO_2, BC and NO_x have the potential for significant climate impacts looking out to 2050. Short-lived species, unlike the long-lived GHGs, do not accumu-

late, so the full impact of short-lived species at 2050 depends on their emissions near that year. At this time, there is very limited quantitative skill in forecasts of emissions of short-lived out to 2050. In fact, it is not clear that we can predict the sign of the change for BC over the next decade. This is a problem that requires not just enhanced scientific knowledge, but also the ability to predict social, economic and technological developments as far as 50 years into the future. One needs only to think back to 1957 to realize how difficult that is and will be.

[76] The emission issues discussed above become even more problematical when the future distributions employed in the AOGCMs are generated by multiple global chemical transport models, all with differing treatments of boundary layer mixing, sub-grid scale transport, large scale transport, wet and dry removal, and atmospheric chemistry and aerosols. The net result is that at this time we cannot find a consensus on the duration, magnitude or even sign of the climate change due to future levels of the short-lived species. However, we have presented a plausible case for enhanced climate warming due to air quality policies that focus primarily on sulfate aerosol reduction (allowing ozone and perhaps BC to increase) as realized in the A1B scenario. Alternative versions of the A1B scenario that follow different pollution control storylines would have alternate impacts.

[77] It is clear that the short-lived species have the potential to play a substantial role in future climate change. Thus it is vital that research continues to provide a better understanding of the climate/air quality linkages so that the decisions policy makers take over the coming decades to address these two societal concerns can be optimized for maximum improvement in both areas.

[78] **Acknowledgments.** We thank Alice Gilliland and Anne Waple for comments, Sara Veasey and Howard Teich for technical support, and especially Ants Leetmaa for inspiring this study. JFL would like to acknowledge L. Buja and H. Tang for their help in running CCSM and analyzing the results. JFL was supported by the SciDAC project from the Department of Energy. The National Center for Atmospheric Research is operated by the University Corporation for Atmospheric Research under sponsorship of the National Science Foundation. We also thank our colleagues at GISS, GFDL and NCAR for their help in creating the models used here.

References

Bauer, S. E., and D. Koch (2005), Impact of heterogeneous sulfate formation at mineral dust surfaces on aerosol loads and radiative forcing in the Goddard Institute for Space Studies general circulation model, *J. Geophys. Res.*, *110*, D17202, doi:10.1029/2005JD005870.

Bauer, S. E., M. I. Mishchenko, A. Lacis, S. Zhang, J. Perlwitz, and S. M. Metzger (2006), Do sulfate and nitrate coatings on mineral dust have important effects on radiative properties and climate modeling?, *J. Geophys. Res.*, *112*, D06307, doi:10.1029/2005JD006977.

Berntsen, T. K., J. S. Fuglestvedt, M. M. Joshi, K. P. Shine, N. Stuber, M. Ponater, R. Sausen, D. A. Hauglustaine, and L. Li (2005), Response of climate to regional emissions of ozone precursors: Sensitivities and warming potentials, *Tellus, Ser. B*, *57*, 283–304.

Boer, G., and B. Yu (2003), Climate sensitivity and response, *Clim. Dyn.*, *20*, 415–429.

Brasseur, G. P., D. A. Hauglustaine, S. Walters, P. J. Rasch, J.-F. Müller, C. Granier, and X. Tie (1998), MOZART, a global chemical transport model for ozone and related chemical tracers, 1. Model description, *J. Geophys. Res.*, *103*(D21), 28,265–28,289.

Collins, W. D., P. J. Rasch, B. E. Eaton, B. Khattatov, J.-F. Lamarque, and C. S. Zender (2001), Simulating aerosols using a chemical transport model with assimilation of satellite aerosol retrievals: Methodology for INDOEX, *J. Geophys. Res.*, *106*(D7), 7313–7336.

Collins, W. D., et al. (2006), The formulation and atmospheric simulation of the Community Atmosphere Model: CAM3, *J. Clim.*, *19*, 2144–2161.

Cooke, W. F., C. Liousse, H. Cachier, and J. Feichter (1999), Construction of a 1-deg × 1-deg fossil fuel emission data set for carbonaceous aerosol and implementation and radiative impact in the ECHAM4 model, *J. Geophys. Res.*, *104*(D18), 22,137–122,162.

Delworth, T. L., et al. (2006), GFDL's CM2 Global Coupled Climate Models. Part I: Formulation and simulation characteristics, *J. Clim.*, *19*, 643–674.

Dentener, F. D., D. S. Stevenson, J. Cofala, R. Mechler, M. Amann, P. Bergamaschi, F. Raes, and R. G. Derwent (2005), Tropospheric methane and ozone in the period 1990–2030: CTM calculations on the role of air pollutant and methane emissions controls, *Atmos. Chem. Phys.*, *5*, 1731–1755.

Fan, S.-M., L. W. Horowitz, H. Levy, and W. J. Moxim (2004), Impact of air pollution on wet deposition of mineral dust aerosols, *Geophys. Res. Lett.*, *31*, L02104, doi:10.1029/2003GL018501.

Fiore, A. M., D. Jacob, B. Field, D. G. Streets, S. D. Fernandes, and C. Jang (2002), Linking ozone pollution and climate change: The case for controlling methane, *Geophys. Res. Lett.*, *29*(19), 1919, doi:10.1029/2002GL015601.

Garrett, T. J., and C. Zhao (2006), Increased Arctic cloud longwave emissivity associated with pollution from mid-latitudes, *Nature*, *440*, 787–789.

Ginoux, P., L. W. Horowitz, V. Ramaswamy, I. V. Geogdzhayev, B. N. Holben, G. Stenchikov, and X. Tie (2006), Evaluation of aerosol distribution and optical depth in the Geophysical Fluid Dynamics Laboratory coupled model CM2.1 for present climate, *J. Geophys. Res.*, *111*, D22210, doi:10.1029/2005JD006707.

Gultepe, I., and G. A. Isaac (1999), Scale effects on averaging cloud droplet and aerosol number concentrations: Observations and models, *J. Clim.*, *12*, 1268–1279.

Hansen, J., and L. Nazarenko (2004), Soot climate forcing via snow and ice albedos, *Proc. Natl. Acad. Sci.*, *101*, 423–428, doi:410.1073/pnas.2237157100.

Hansen, J., M. Sato, R. Ruedy, A. Lacis, and V. Oinas (2000), Global warming in the twenty-first century: An alternative scenario, *Proc. Natl. Acad. Sci.*, *97*, 9875–9880.

Hansen, J., et al. (2005), Efficacy of climate forcings, *J. Geophys. Res.*, *110*, D18104, doi:10.1029/2005JD005776.

Hansen, J., et al. (2007), Dangerous human-made interference with climate: A GISS modelE study, *Atmos. Chem. Phys.*, *7*, 2287–2312.

Held, I. M., and B. J. Soden (2006), Robust responses of the hydrological cycle to global warming, *J. Clim.*, *19*(21), 5686–5699.

Horowitz, L. W. (2006), Past, present, and future concentrations of tropospheric ozone and aerosols: Methodology, ozone evaluation, and sensitivity to aerosol wet removal, *J. Geophys. Res.*, *111*, D22211, doi:10.1029/2005JD006937.

Horowitz, L. W., et al. (2003), A global simulation of tropospheric ozone and related tracers: Description and evaluation of MOZART, version 2, *J. Geophys. Res.*, *108*(D24), 4784, doi:10.1029/2002JD002853.

Intergovernmental Panel on Climate Change (2007), *Climate Change 2007: The Scientific Basis*, Cambridge Univ. Press, New York.

Jacobson, M. Z. (2004), Climate response of fossil fuel and biofuel soot, accounting for soot's feedback to snow and sea ice albedo and emissivity, *J. Geophys. Res.*, *109*, D21201, doi:10.1029/2004JD004945.

Kiehl, J. T., J. J. Hack, G. B. Bonan, B. A. Boville, D. L. Williamson, and P. J. Rasch (1998), The National Center for Atmospheric Research Community Climate Model: CCM3, *J. Clim.*, *11*, 1131–1149.

Kiehl, J. T., T. L. Schneider, R. W. Portmann, and S. Solomon (1999), Climate forcing due to tropospheric and stratospheric ozone, *J. Geophys. Res.*, *104*(D24), 31,239–31,254.

Kinne, S., et al. (2006), An AeroCom initial assessment – Optical properties in aerosol component modules of global models, *Atmos. Chem. Phys.*, *6*, 1815–1834.

Koch, D., G. Schmidt, and C. Field (2006), Sulfur, sea salt and radionuclide aerosols in GISS ModelE, *J. Geophys. Res.*, *111*, D06206, doi:10.1029/2004JD005550.

Koch, D., T. Bond, D. Streets, N. Bell, and G. R. van der Werf (2007), Global impacts of aerosols from particular source regions and sectors, *J. Geophys. Res.*, *112*, D02205, doi:10.1029/2005JD007024.

Lamarque, J.-F., P. Hess, L. Emmons, L. Buja, W. M. Washington, and C. Granier (2005), Tropospheric ozone evolution between 1890 and 1990, *J. Geophys. Res.*, *110*, D08304, doi:10.1029/2004JD005537.

Levy, H., M. D. Schwarzkopf, L. Horowitz, and V. Ramaswamy (2008), Anthropogenic short-lived radiative species at the intersection of climate and air quality, in press.

Madronich, S., and S. Flocke (1998), The role of solar radiation in atmospheric chemistry, in *Handbook of Environmental Chemistry*, edited by P. Boule, pp. 1–26, Springer-Verlag, New York.

Menon, S. A., D. Del Genio, D. Koch, and G. Tselioudis (2002), GCM simulations of the aerosol indirect effect: Sensitivity to cloud parameterization and aerosol burden, *J. Atmos. Sci.*, *59*, 692–713.

Miller, R. L., et al. (2006a), Mineral dust aerosols in the NASA Goddard Institute for Space Studies ModelE AGCM, *J. Geophys. Res.*, *111*, D06208, doi:10.1029/2005JD005796.

Miller, R. L., G. A. Schmidt, and D. T. Shindell (2006b), Forced variations of annular modes in the 20th century intergovernmental panel on climate change fourth assessment report models, *J. Geophys. Res.*, *111*, D18101, doi:10.1029/2005JD006323.

Mitchell, J. F. B., R. A. Davis, W. J. Ingram, and C. A. Senior (1995), On surface temperature, greenhouse gases, and aerosols: Models and observations, *J. Clim.*, *8*, 2364–2386.

Nakicenovic, N., et al. (2000), *IPCC Special Report on Emissions Scenarios*, 570 pp., Cambridge Univ. Press, Cambridge, U. K.

Olivier, J. G. J., and J. J. M. Berdowski (2001), Global emissions sources and sinks, in *The Climate System*, edited by J. Berdowski et al., pp. 33–78, A. A. Balkema Publishers/Swets and Zeitlinger Publishers, Lisse, Netherlands.

Penner, J. E., J. Quaas, T. Storelvmo, T. Takemura, O. Boucher, H. Guo, A. Kirkevag, J. E. Kristjansson, and Ø. Seland (2006), Model intercomparison of indirect aerosol effects, *Atmos. Chem. Phys. Discuss.*, *6*, 1579–1617.

Schmidt, G. A., et al. (2006), Present day atmospheric simulations using GISS ModelE: Comparison to in-situ, satellite and reanalysis data, *J. Clim.*, *19*, 153–192.

Schulz, M., et al. (2006), Radiative forcing by aerosols as derived from the AeroCom present-day and pre-industrial simulations, *Atmos. Chem. Phys.*, *6*, 5225–5246.

Shindell, D. T., G. Faluvegi, N. Bell, and G. A. Schmidt (2005), An emissions-based view of climate forcing by methane and tropospheric ozone, *Geophys. Res. Lett.*, *32*, L04803, doi:10.1029/2004GL021900.

Shindell, D. T., G. Faluvegi, A. Lacis, J. E. Hansen, R. Ruedy, and E. Aguilar (2006a), The role of tropospheric ozone increases in 20th century climate change, *J. Geophys. Res.*, *111*, D08302, doi:10.1029/2005JD006348.

Shindell, D. T., G. Faluvegi, N. Unger, E. Aguilar, G. A. Schmidt, D. Koch, S. E. Bauer, and R. L. Miller (2006b), Simulations of preindustrial, present-day, and 2100 conditions in the NASA GISS composition and climate model G-PUCCINI, *Atmos. Chem. Phys.*, *6*, 4427–4459.

Shindell, D. T., G. Faluvegi, S. E. Bauer, D. M. Koch, N. Unger, S. A. Menon, R. L. Miller, G. A. Schmidt, and D. G. Streets (2007), Climate response to projected changes in short-lived species under an A1B scenario from 2000–2050 in the GISS climate model, *J. Geophys. Res.*, *112*, D20103, doi:10.1029/2007JD008753.

Stewart, R. W., S. Hameed, and J. P. Pinto (1977), Photochemistry of the tropospheric ozone, *J. Geophys. Res.*, *82*(21), 3134–3140.

Streets, D., T. C. Bond, T. Lee, and C. Jang (2004), On the future of carbonaceous aerosol emissions, *J. Geophys. Res.*, *109*, D24212, doi:10.1029/2004JD004902.

West, J. J., and A. M. Fiore (2005), Management of tropospheric ozone by reducing methane emissions, *Environ. Sci. Technol.*, *39*, 4685–4691.

G. Faluvegi and D. T. Shindell, NASA Goddard Institute for Space Studies, Center for Climate Systems Research, Columbia University, 2880 Broadway, New York, NY 10025, USA. (dshindell@giss.nasa.gov)

L. W. Horowitz, H. Levy II, and M. D. Schwarzkopf, GFDL/NOAA, Princeton University, P.O. Box 308, Princeton, NJ 08542-0308, USA.

J.-F. Lamarque, Atmospheric Chemistry Division, National Center for Atmospheric Research, P.O. Box 3000, Boulder, CO 80307-3000, USA.